Origami with negative refractive index to generate super-lenses

Fanny Guenneau, Sangeeta Chakrabarti, Sébastien Guenneau, S. Anantha Ramakrishna

Origami with negative refractive index to generate super-lenses

Fanny Guenneau[1], Sangeeta Chakrabarti[1,2], Sebastien Guenneau[1] and S Anantha Ramakrishna[3]

[1] Aix-Marseille Université, CNRS, Centrale Marseille, Institut Fresnel, 13013 Marseille, France
[2] Department of Physics and Astronomy, University of California, Irvine, California 92697, USA
[3] Department of Physics, Indian Institute of Technology, Kanpur 208016, India

E-mail: sebastien.guenneau@fresnel.fr and sar@iitk.ac.in

Abstract

Negative refractive index materials (NRIM) enable unique effects including superlenses with a high degree of sub-wavelength image resolution, a capability that stems from the ability of NRIM to support a host of surface plasmon states. Using a generalized lens theorem and the powerful tools of transformational optics, a variety of focusing configurations involving complementary positive and negative refractive index media can be generated. A paradigm of such complementary media are checkerboards that consist of alternating cells of positive and negative refractive index, and are associated with very singular electromagnetics. We present here a variety of multi-scale checkerboard lenses that we call *origami* lenses and investigate their electromagnetic properties both theoretically and computationally. Some of these meta-structures in the plane display thin bridges of complementary media, and this highly enhances their plasmonic response. We demonstrate the design of three-dimensional checkerboard meta-structures of complementary media using transformational optics to map the checkerboard onto three-dimensional corner lenses, the only restriction being that the corresponding unfolded structures in the plane are constrained by the four color-map theorem.

Keywords: negative refraction, super lens, checkerboard

(Some figures may appear in colour only in the online journal)

1. Introduction

Materials with simultaneously negative dielectric permittivity (ε) and magnetic permeability (μ) can be said to have negative refractive index [1–3]. Light incident from positive media on a flat interface with such materials refracts 'oppositely' onto to the same side of the normal and such interfaces can support surface electromagnetic modes for both polarizations of light [3]. When $\varepsilon = -1$ and $\mu = -1$, all the surface electromagnetic modes become degenerate and a flat slab of such material behaves as a perfect lens [4]. Evanescent modes associated with object features at all subwavelength lengthscales are involved in the imaging process through the excitation of surface plasmon modes on the slab's surfaces. The image formed is, in principle, perfect with no limitation on the image resolution. Straight forward implementation of this idea is difficult due to the practical limitations of obtaining materials with $\varepsilon = -1$ and $\mu = -1$ exactly. If nothing else, absorption of light in the lens material becomes a major spoiler and limits the extent of subwavelength resolution obtainable [5]. Designer structured composite materials, popularly known as metamaterials, have been shown to have negative refractive index from microwave frequencies almost into the visible frequencies [2, 6–8]. The spatial size of the unit cell of the metamaterial ultimately limits the image resolution. Plasmonic materials with negative dielectric permittivity, such as silver and gold, were also suggested for use as super-lenses as they mimic the action of NRIM for one polarization of light at very small lengthscales, [4].

The idea of the perfect lens was generalized to spatially inhomogeneous media [9], whereby it was realized that the volume of two slabs of material are equivalent to null space if their material parameters are given by

$$\begin{aligned} \varepsilon_1 &= +\varepsilon(x, y, -z), \quad \mu_1 = +\mu(x, y, -z), \quad -d < z < 0, \\ \varepsilon_2 &= -\varepsilon(x, y, z), \quad \mu_2 = -\mu(x, y, z), \quad 0 < z < d. \end{aligned} \tag{1}$$

In other words, the transverse variation does not matter as long as it is the same in both slabs and the interface between the two slabs should be a plane of mirror anti-symmetry. The electromagnetic fields on the $z = -d$ plane are simply transferred and reproduced on the $z = d$ plane. Thus to an observer on the right, it appears as if the region in $-d < z < d$ does not exist. The complementary slabs optically 'cancel' each other's presence for both evanescent as well as propagating modes. Thus, an incident plane wave suffers no change in amplitude or in phase upon traversal through the complementary medium pair. There is a perfect one-to-one imaging and the perfect focus will occur irrespective of the medium in which the complementary medium pair is embedded. The most general conditions for the perfect imaging can include anisotropic materials [9] and bianisotropic materials [10].

Checkerboards consisting of alternate regions of positive and negative index media are interesting examples of complementary media [11–13]. Predictions of a ray picture and the generalized perfect lens conclusions can often be at loggerheads [12, 14]. A complementary layer pair composed of triangular cells arranged in checkerboard fashion [13] exemplifies situations whereby the ray picture can predict zero transmittance while the above theorem assures us of perfect transmittance. These are examples of extraordinary transmission mediated by excitation and scattering of surface plasmon waves via the corners. The mechanism of plasmonic guidance involved here differs substantially from the extraordinary transmission through subwavelength holes in opaque metallic films [15, 16].

A corner (wedge) made of negative refractive index material shares the perfect imaging property of other negatively refracting lenses [9]. A pair of negatively refracting corners with $\epsilon = -1$ and $\mu = -1$ is capable of bending light in a loop and forming a series of images such that the light circulates within the loop forever (see figure 1). A checkerboard is essentially a large collection of periodically placed corners between positive and negative refractive media, where the corners and edges are expected to dominate all the photonic properties of the checkerboards. In infinite non-absorptive checkerboard lattices, a source placed in one cell of the checkerboard produces an image in every other cell [11]. In the absence of dissipation, infinite lattices of such checkerboard systems are very singular, and only the idea of complementary media can be used to deduce anything useful. Apart from such theoretically esoteric properties, checkerboards potentially have many useful properties: for example, a finite checkerboard of triangular cells with adjacent triangles having refractive index, $n = \pm 1$, has been suggested to strongly confine light [13], while plasmonic nano-checkerboards of gold have been shown to support broadband extraordinary transmission of light [17]. However, as illustrated by the paradoxes of the intuitive, but approximate, ray picture showing no transmission and the complementary theorem showing perfect transmission, it becomes imperative to investigate numerically the full wave solutions of finite checkerboard structures of NRIM to understand their properties. Dissipation is also known to affect sub-wavelength imaging badly, and the large local field enhancements can only worsen the situation. It is due to this fact that the effect of dissipation on sub-wavelength imaging becomes an important issue.

The purpose of this paper is three-fold:

- We present here new kinds of checkerboard-like complementary media composed of piece-wise continuous areas that we call 'origami' lenses. These novel configurations give rise to interesting new possibilities for plasmonic materials and interactions. Certain forms of Origami lenses can have thin bridge structures. A homogenization analysis for such structures exemplifies the singular plasmonic properties.
- We generalize the ideas of two dimensional checkerboard systems to three dimensions using the powerful techniques of geometrical transformations and show how the tiling should obey the famous *four color-map* theorem.
- The nuances and sensitivities of numerical simulations of checkerboard configurations are investigated using two spectral methods: the finite element method using the COMSOL software and the transfer matrix method. It turns out that accurate modelling of a checkerboard structure can be a litmus test of the numerical programs and meshing.

The paper is organized into sections elaborating upon the above points.

2. Origami lenses

There is a crystallographic restriction that rotational symmetries in planar crystals are limited to two-fold, three-fold, four-fold, and six-fold. Further, keeping a balance between overall positive refractive index material and NRIM implies that we are only left with checkerboards of either rectangular, square or (equilateral) triangular cells. Nevertheless, one might look for other ways of tiling the plane such that the unit cell can have further structure, which respects the mirror-antisymmetry conditions as well as the crystallographic conditions. We show examples of structured unit cells in figure 1 that have an overall balance of positive and negative complementary media so that the unit cell overall has zero optical path-length. Such designs are reminescent of Victor Vasarely's art where checkerboards have been used to great effect[4]. We term such lenses as *origami lenses* and study them principally due to curiosity. It turns out that such lenses have very interesting electromagnetic properties that we present in the sequel.

For reference, we first present the results for the perfect lens and for the *poor man's* silver lens with super-resolution. We show in figure 2, the results of finite element computations

[4] Some of the paintings can be found on the official webpage of Victor Vasarely www.vasarely.com.

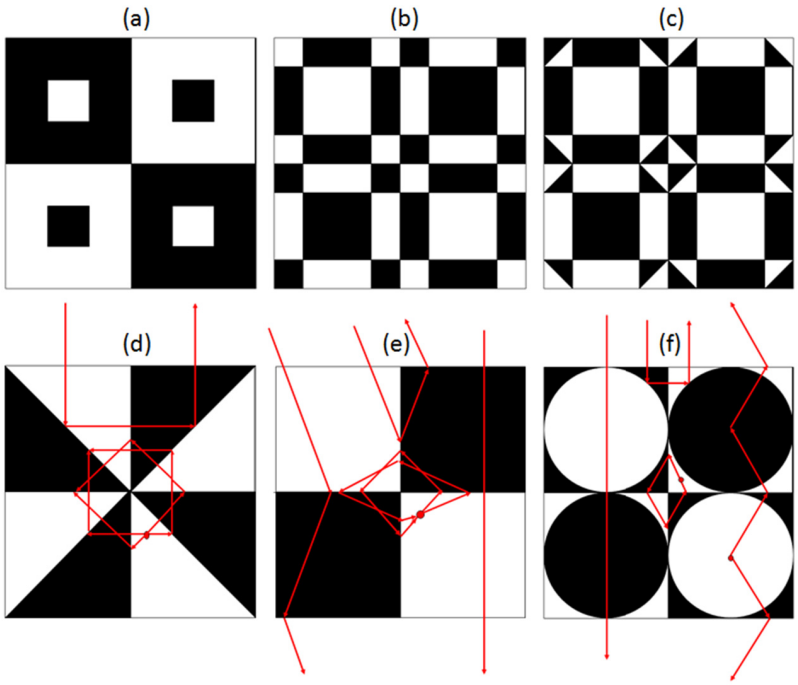

Figure 1. Several possibilities for origami lenses are shown with various geometric shapes. The principle is that equal regions of media with opposite signs of refractive index have to be placed on either side of the central plane so that the anti-symmetry conditions of equation (1) are satisfied, a condition which is met in (a)–(f). If white represents a region with $n = 1$, then black represents a region with $n = -1$. Typical ray trajectories are shown in (d)–(f).

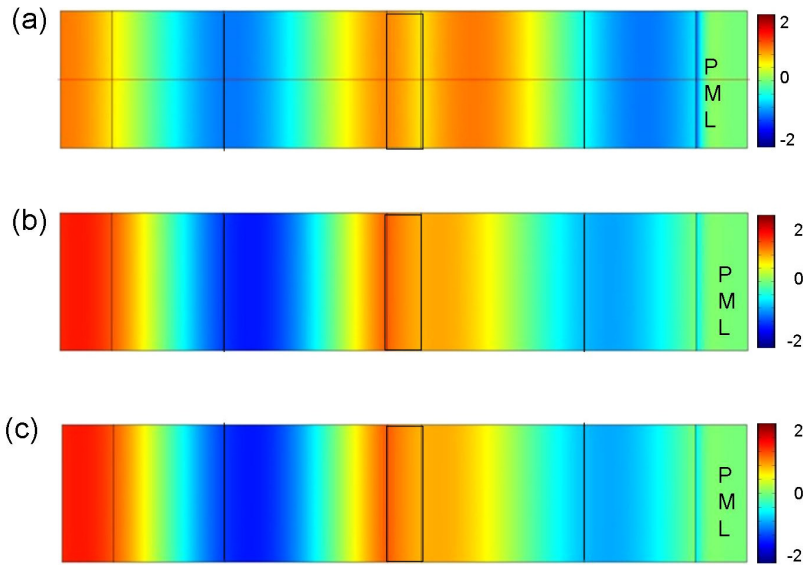

Figure 2. A rectangular slab lens with; (a) $\varepsilon = \mu = -1$; (b) $\varepsilon = -1 + i0.01$, $\mu = +1$; (c) $\varepsilon = -1 + i0.1$, $\mu = +1$, illustrating the transmission of a plane wave incident from the left. The results shown are for p-polarized light and thickness of the lens $d \simeq \lambda/10$.

implemented using the for a planewave incident on a slab lens of infinite extent along the transverse direction. P-polarized (TM) radiation is incident from the left on the slab with width $d = \lambda/10$. In figure 2, the transmission properties of three types of slab lens has been illustrated: (a) the perfect slab lens with $\varepsilon = \mu = -1$; (b) a dissipative negative dielectric superlens with $\varepsilon = -1 + i0.01$, $\mu = 1$; and (c) a more dissipative negative dielectric slab with $\varepsilon = -1 + i0.1$, $\mu = 1$. Perfect transmission is obtained in figure 2(a) and this is seen to decrease in figures 2(b) and (c). These results have been summarized in table 1 below.

We then add some complementary media within the slab lens, see figures 3–6. The complementary lens regions in figure 3 has rectangular inclusions of media with opposite signs, the ones in figures 4 and 5 have inclusions of triangular shape, while the ones in figure 6 has circular inclusions with square or rectangular regions. A p-polarized plane wave is assumed

Table 1. Transmission (in percent) through checkerboard slab lens with embedded regions of different configurations for various values of material parameters.The last column shows the transmission that would have been obtained had a silver slab lens been used for imaging. The slab lens is seen to be the most efficient, while transmissions greater than 40% are obtained for the triangular inclusions, where no light is expected to be transmitted. The origami lens with circular inclusions shows a dramatic reduction in transmission, and transmits very little radiation, in close correspondence with its behaviour as predicted by ray diagrams, but in contradiction with the generalized lens theorem. The transmittances slightly greater than 100% can be attributed to the lack of convergence of the calculations.

NRM checkerboard lens	$\varepsilon = \mu = -1$	$\varepsilon = -1 + i * 0.01$
Slab lens	100	99.3
Embedded rectangles (□) (figure 1, left)	100	82.3
Triangular(△) (figure 5)	100	77.5
Triangular(▽) (figure 4)	100.1	67.7
Embedded circle (○)(figure 6)	100.2	4.963
NRM checkerboard lens	$\varepsilon = -1 + i * 0.1$	$\varepsilon = -1 + i * 0.4$
Slab lens	92.5	75.4
Embedded rectangles (□) (figure 1, left)	69.9	55.3
Triangular(△) (figure 5)	62	45.3
Triangular(▽) (figure 4)	55.6	42.2
Embedded circle (○)(figure 6)	2.62	1.86

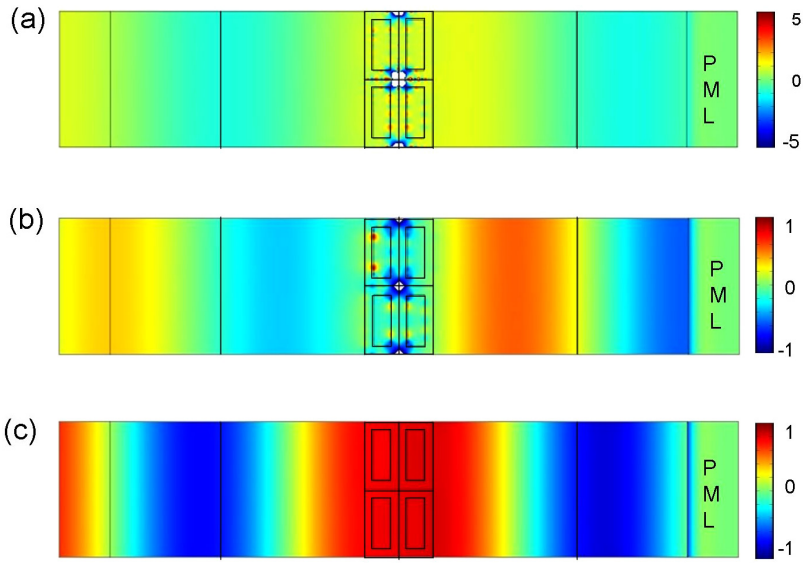

Figure 3. Origami lens with embedded rectangular cells; (*a*) $\varepsilon = \mu = -1$; (*b*) $\varepsilon = -1 + i0.01$; (*c*) $\varepsilon = -1 + i0.1$. A plane wave is incident from the left and transmitted across the slab. The results are for p-polarized light and the thickness of the checkerboard $d \simeq \lambda/5$.

to be normally incident from the left. In all these cases studied, the width of the checkerboard $d \simeq \lambda/10$. We solve the Maxwell system using Finite Edge Elements (also known as Whitney forms) which naturally fulfill ordinary conditions for the tangential components of the electromagnetic field at interfaces between positive and negative index media (hence exhibiting two anti-parallel wave-vectors at both sides of such interfaces) [12, 19]. Outgoing wave conditions ensuring well-posedness of the problem (existence and uniqueness of the solution) are enforced through implementation of Berenger Perfectly Matched Layers within the rightmost rectangular domain [18]. While the expression of the incident plane wave is enforced on the leftmost boundary, the field is set to be zero on the rightmost boundary, and periodic boundary conditions are in order on the top and bottom walls to simulate an infinite array in the transverse vertical direction. The transmission through the line integral of the scattered fields is computed on the two vertical lines located halfway from the checkerboard and the boundaries (left and right).

Note that in each of these cases, there is overall balance between regions with positive and negative media and also the mirror anti-symmetry conditions for the generalized perfect lens system are respected. While the electromagnetic fields are clearly enhanced within the perfect origami lens regions, the plane-wave still transmits in an unperturbed manner with unit transmission as the overall amount of positive and negative index media is well balanced. Note that once we have $\mu = 1$ for the negative dielectric lens cases, the nice phase compensation seen for the plane wave is lost. These complementary media pairs provide a reflectionless interface between the region of interest (a large middle square containing the line source and the silver checkerboard on figure 3) and the PML (four elongated rectangles and four small squares) at all incident angles. It is obvious from figures 4–6 that both the rectangular and triangular checkerboards enable an imaging process in full contradiction with the ray picture. Extraordinary transmission is at work! There is a large localization of electromagnetic fields along the interfaces between positive

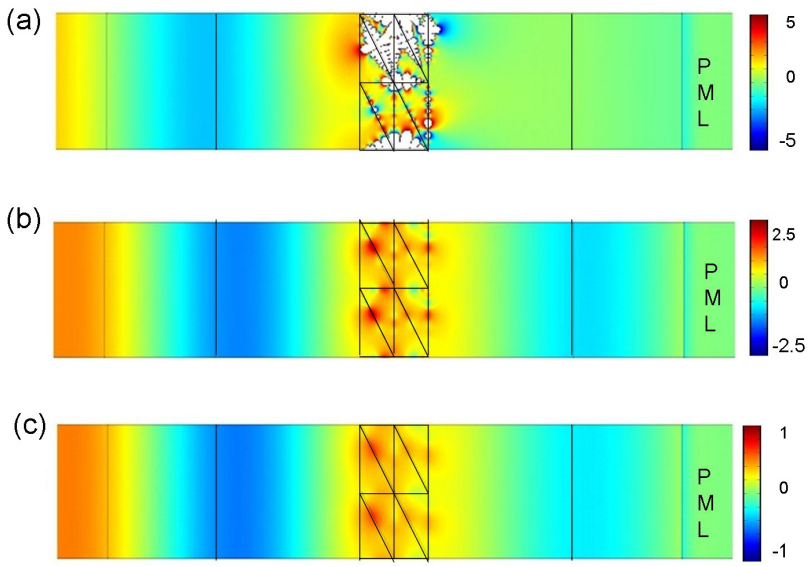

Figure 4. Origami lens with right-angled triangular cells; (*a*) $\varepsilon = \mu = -1$; (*b*) $\varepsilon = -1 + i0.01$; (*c*) $\varepsilon = -1 + i0.1$. As before, each of these figures illustrates the transmission of a plane wave incident from the left hand side, for p-polarized light across a slab whose thickness $d \simeq \lambda/5$.

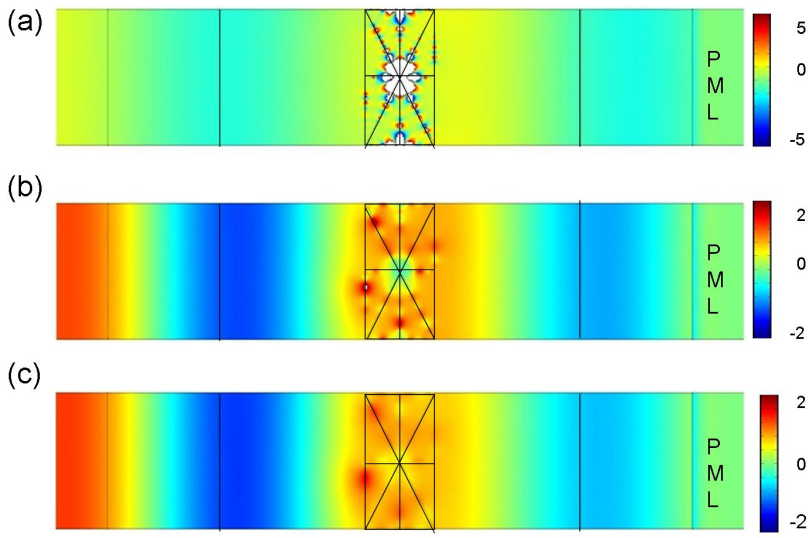

Figure 5. Origami lens with triangular cells arranged in a different pattern for (*a*) $\varepsilon = \mu = -1$; (*b*) $\varepsilon = -1 + i0.01$; (*c*) $\varepsilon = -1 + i0.1$. Evidently, the field distributions and the transmission, obtained for a p-polarized plane wave incident from the left, are quite different from the ones shown in figure 4. As before, the thickness of the slab, $d \simeq \lambda/5$.

and negative media, which depend upon the symmetry of the systems under consideration. This is exemplified by figures 5 and 6 where we find enormous fields across several interfaces for the complementary media pairs.

The numerical calculations shown in figures 3–6 also showcase the response of the origami lenses with increasing dissipation. Dissipation is seen to affect these checkerboards, particularly the ones with embedded triangular and circular inclusions. The results obtained for the transmission characteristics of such checkerboards, have been summarized in table 1. It is illuminating to interpret the data using either of the ray or the wave optical viewpoints: the former tells us that 50% of rays should be transmitted through the rectangular checkerboard lens, whereas all rays should be reflected for the triangular checkerboard lens. On the contrary, the generalized lens theorem states that any such checkerboard lens has a full transmission in the limit of no dissipation. This wave picture is indeed fully adequate for the ideal case whereby $\varepsilon = \mu = -1$ in the NRIM, as exemplified by the first column of table 1. However, the situation becomes different when we introduce some dissipation in the NRIM: The transmission for incident propagating plane-waves hardly exceeds 50% for rectangular and triangular checkerboard silver lenses, as reported in the last column of table 1. Interestingly, the case of a checkerboard lens with embedded cylinders as in figure 6 is drastically affected by dissipation: even a small level of absorption leads to a dramatic drop in the transmittance, with less than 2% of light passing through such a silver lens (in contradistinction with the generalized lens theorem, but in agreement with the ray picture). This is undoubtedly due to the very large number

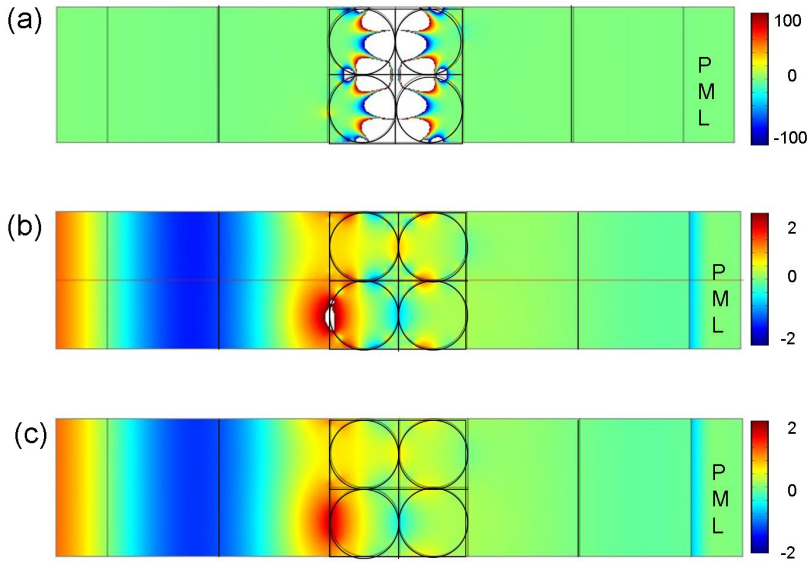

Figure 6. Origami lens with embedded cylindrical cells for (a) $\varepsilon = \mu = -1$; (b) $\varepsilon = -1 + i0.01$; (c) $\varepsilon = -1 + i0.1$. The transmission and the field distributions for a p-polarized plane wave incident from the left on a checkerboard slab $d \simeq \lambda/5$ (as in the preceding figures) have been shown. The white regions indicate large fields that are larger and beyond the color-map range.

of resonances that can be excited in systems of touching cylinders and spheres [20]. The transmittances can, however, be large for evanescent plane waves due to the intense coupling to the surface plasmons on the interfaces between the positive and negative media.

Such a counter-example for the application of the perfect lens theorem to dissipative NRIM should warn us that the behaviour of structured perfect lenses with thin-bridges within which oscillations of the electromagnetic field are tremendously enhanced, cannot be fully predicted. Numerical simulations should take into account the strongly enhanced local fields. The reason for that is very simple: The interstitial space between the disks can be modelled as a large curved rhombus-like structure (see figure 7) connected to four thin domains $\Pi_\eta = \{\mathbf{x} \in \mathbb{R}^2 : l/2 < x_1 < l/2, \eta h_-(x_1) < x_2 < \eta h_+(x_1)\}$ (see figure 7). Assuming that either the electric or magnetic field is orthogonal to the plane, the Maxwell equations for a time harmonic wave with angular frequency ω and phase velocity c, reduce to

$$\nabla^2 u + \omega^2/c^2 u = 0, \tag{2}$$

in each homogenous region (shown in black and white in the figure) of the bridge, the boundary conditions on the fields at the interface between these regions as well as on the upper and lower boundaries h_- and h_+ of Π_η is given by the continuity of u and a negative jump of its normal derivative i.e. $[u] = 0$ and $[\mathrm{d}u/\mathrm{d}n] = -1$. Assuming the following ansatz for u:

$$u \sim u_0(x_1) + \eta^2 u_1(x_1, \xi) \tag{3}$$

where $\xi = x_2/\eta$ and the rescaled gradient

$$\nabla = \nabla_{x_1} + \frac{1}{\eta}\nabla_\xi \ , \tag{4}$$

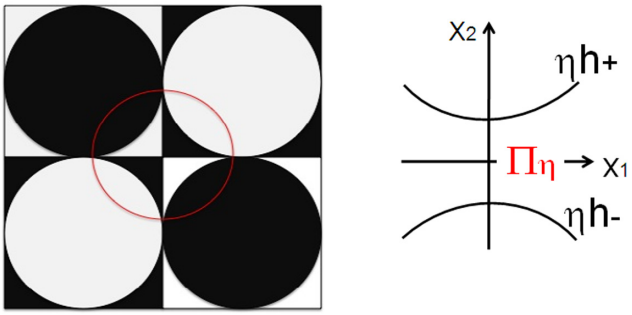

Figure 7. Schematic diagram of the checkerboard with embedded circles, with the interstitial region highlighted in red (left). The interstitial space has been modelled as a large curved diamond-shaped region connected to four thin domains: these are curved ligaments Π_η bounded by two functions $h_\pm$ scaled by a small parameter η (right).

the Helmholtz equation is reduced to an ordinary differential equation for $-l/2 < x_1 < l/2$ at the leading order:

$$\frac{\mathrm{d}}{\mathrm{d}x_1}\left((h_+(x_1) + h_-(x_1))\frac{\mathrm{d}}{\mathrm{d}x_1}u_0\right) + \omega^2/c^2(h_+(x_1) + h_-(x_1))u_0 = 0. \tag{5}$$

This equation is supplied with boundary conditions at the endpoints $x_1 = \pm l/2$. Such boundary conditions can be easily derived from the divergence theorem applied to the flux through the interface between each thin bridge Π_η and the large region Σ to which they are connected. In the case of constant curvature a, that is when $h_- = h_+ = 1 + a^2h^2/2$, this leads the following resonant frequency (see equation (4.12) in [21]):

$$\omega \sim 2\eta^2 \frac{c^2}{\mathrm{area}(\Sigma)} \frac{ah}{\arctan(al/2)} \ . \tag{6}$$

Compared to the earlier work in [21], such resonant frequencies are highly degenerate in the present case. In the

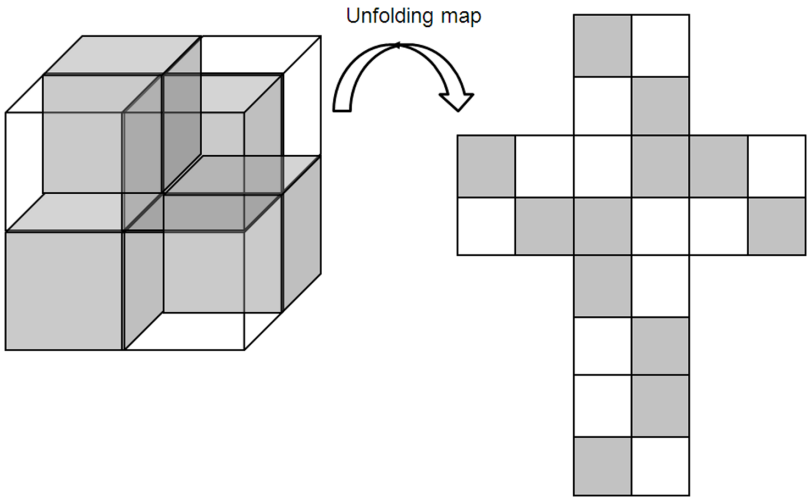

Figure 8. Left: unit cell for a three-dimensional two-phase periodic checkerboard consisting of cubes filled with positive (white) and negative (grey) refractive index media. Right: unfolded checkerboard exemplifying the role of symmetries and rotations in the design. Interfaces between cubes (i.e. faces and edges) support a host of surface and edge plasmons.

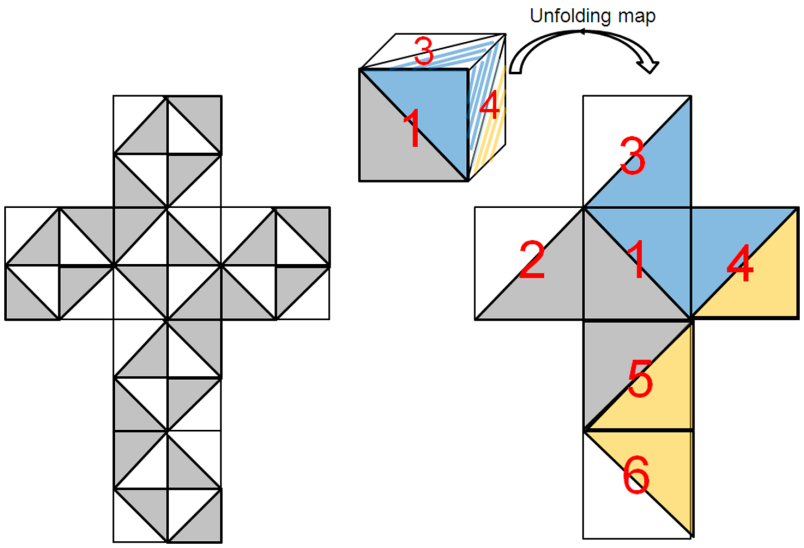

Figure 9. Left: unfolded checkerboard consisting of right-angled tetrahedra filled with positive (white) and negative (grey) refractive index media. This leads to an impossible three-dimensional checkerboard. Right: elementary brick of a four phase three-dimensional checkerboard (see figure 10) with its unfolded counterpart consisting of four complementary phases. These negative and positive results are consistent with the four color theorem.

limit of zero dissipation in NRIM for the balanced Origami lenses, area (Σ) vanishes and the resonant frequencies ω form a continuum. This leads to a highly resonant structure at any frequency, which is a hallmark of an infinite local density of states.

3. Four color-map theorem applied to 3-D checkerboards of complementary media

It was shown in [11] that it is possible to fold the Euclidean space back onto itself using an alternation of positively and negatively refracting cubic regions. We reproduce in figure 8 the original idea of [11]. The case of 3D origami checkerboards, such as shown in figures 9 and 10 was not considered there. Such checkerboards are more challenging as their design is constrained by the four color-map theorem as we will now show.

In mathematics, the famous four color theorem, or the four color map theorem, established in 1976 by Appel *et al* and Appel and Haken [22, 23] using computational techniques, states that: 'Given any separation of a plane into contiguous regions, producing a figure called a map, no more than four colors are required to color the regions of the map so that no two adjacent regions have the same color. Two regions are called adjacent only if they share a border segment, not just a point.'

In the present case, this theorem warns us that a two-phase three-dimensional checkerboard with intricate patterns might not be possible at all as its design requires to work with unfolded regions in the plane which should not share frontiers,

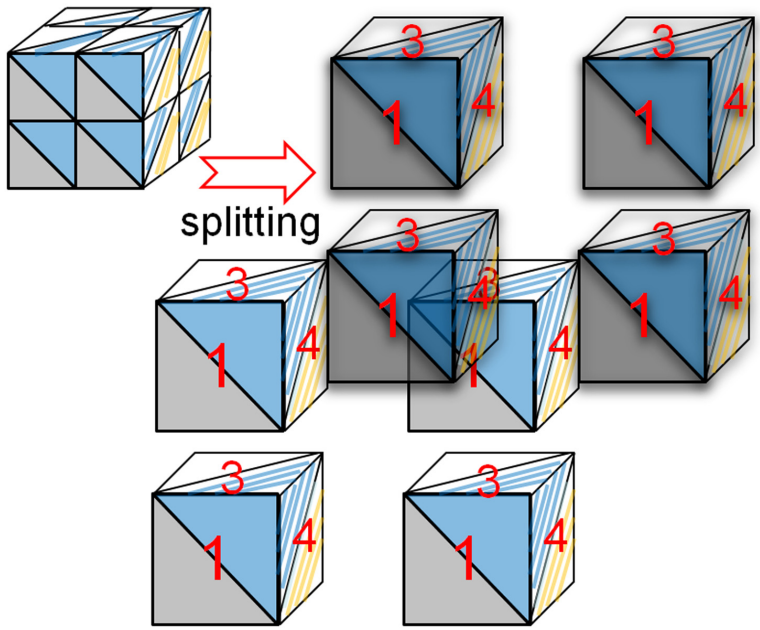

Figure 10. Four phase three-dimensional checkerboard consisting of right-angled tetrahedra filled with positive (white, $n = n_1$, blue $n = n_2$) and negative (grey, $n = -n_1$, yellow, $n = -n_2$) refractive index media.

just like in the four color-map theorem. We are indeed unable to propose any two-phase checkercubes consisting of right-angled tetrahedra, as shown in figures 9 and 10. This is, to the best of our knowledge, the first example of an impossible three-dimensional arrangement of checkercubes in the context of plasmonics.

4. Numerical analysis of checkerboard structures

We have seen it is thus possible to design very complex metamaterials using a very simple group theoretical approach [11], and this already led to the discovery of infinite checkerboards of alternating cells of complementary media. However, a systematic study of such checkerboards is far from being easy, as standard numerical packages such as finite elements might fail to converge in the analysis of such strongly resonant metamaterials, as shown in [12]. Some rigorous mathematical study of such sign-shifting media has been performed by Bonnet-Bendhia and co-workers [19]. It is shown there that the Lax–Milgram lemma does not apply anymore due to lack of ellipticity. But it is still possible to invoke the Fredholm alternative in order to be assured that any numerical solution found by a finite element algorithm satisfying the prerequisite boundary conditions on the interfaces between complementary media and adhoc outgoing wave conditions at infinity (such as Sommerfeld ones) exists in its own right (is not spurious). It was also observed in [12] that the PHOTON code based on the transfer matrix method is an alternative to the standard commercial package COMSOL™ in handling transmission type problems through rectangular checkerboard lenses with or without dissipation. In this section, we explore more intricate checkerboard lenses displaying some thin bridges between complementary media within which the electromagnetic fields are further enhanced. Some paradoxes occur when the checkerboard lens becomes infinite in all-space dimensions: in this case, one has to think of the periodic structure as being born of a torus and any source located within a unit cell will show an infinite number of images in any other cell of the checkerboard (which actually reduces to one cell).

We now examine the response of a NRIM checkerboard lattice lens with finite transverse size, when its unit cells exhibit a four-fold geometry with complex patterns. We note that the case of thin-bridges inclusions within the checkerboard structures represents a singular situation which is very hard to handle with the finite element method.

4.1. Transfer matrix method calculations

The response of some novel checkerboards was calculated using the PHOTON codes based on the transfer matrix method. A schematic representation of such checkerboards has been shown in figure 1, extreme left. These calculations are very sensitive to numerical errors. Accurate calculations for such highly singular structures require a very fine numerical grid. In addition, the regions of opposite index media must have equal thicknesses in order to be optically complementary and satisfy the Generalized Lens theorem. The use of an unsatisfactory numerical grid results in the appearance of numerical artifacts, in the form of resonances at wave vectors $k_x/k_0 \sim 1$, where no resonances are predicted to occur. We have dealt with this issue in [12] and shown that an optimized numerical grid pushes this spurious resonance to $k_x \simeq 3k_0$. If the thicknesses of the adjacent regions of the checkerboards differs even by a small amount, spurious resonances crop up again. Similar effects are observed if a less accurate grid (consisting of 202 points along each dimension) is used or if the adjacent cells of the checkerboard differ by a small fraction (typically 1%) of the wavelength. These are due to spurious resonances caused by

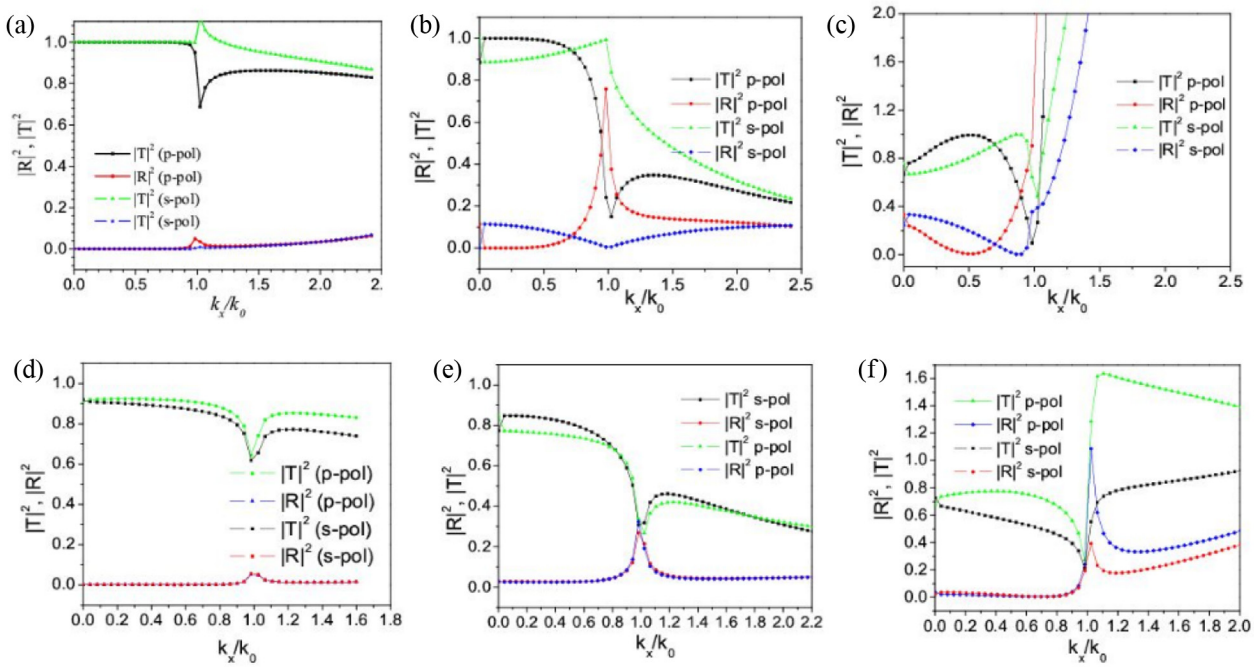

Figure 11. Transfer matrix analysis of the checkerboard structures shown in figure 1 (left) illustrating their transmission properties for s- and p-polarizations. The transmission properties change as the thickness of the embedded regions changes. As the embedded regions become smaller in size, (for the graphs from left to right, top and bottom panels) the transfer matrix calculations begin to show considerable deviations. (a, d) represent the transmission properties of non-dissipative and dissipative checkerboards, respectively, whose embedded regions are fairly large in size. (b, e) illustrate the transmittive properties of non-dissipative and dissipative checkerboards, respectively, whose embedded regions are of intermediate size. (c, f) illustrate the same properties for non-dissipative and dissipative checkerboards with extremely small embedded regions.

the numerical dispersion that almost mimic surface plasmon resonances.

In the upper panel of figure 11, we present the result of our transfer matrix calculations for an optimized grid consisting of 262 points along $\hat{x}$ and 106 points along $\hat{z}$. These media exhibit nearly unit transmittivity and zero reflectivity even for sub-wavelength wave vectors. However, when the embedded regions are very small in size, there appears to be significant deviations from the complementary lens theorem. But this is more likely to be a constraint due to the grid used, rather than implying any actual deviation of the physical behaviour of the system from the complementary behaviour. The transmittivity indicates that the system behaves as predicted by the Generalized Lens theorem. Any small mismatches in the widths of the regions results in the appearance of numerical artifacts. Otherwise, with accurate meshing, near-unit transmittivity and zero reflectivity are obtained.

5. Conclusions

We have presented here an assortment of some surprising configurations of complementary media based perfect lenses that we term as *origami lenses*. Numerical calculations with these lenses, while demonstrating the imaging capabilities, also indicate the presence of enormous localized electromagnetic fields. An application of the four color-map theorem to mappings of checkerboards to 3D systems is shown to put in restrictions on the manner of three dimensional checker-cube systems. The checkerboard configurations also support reasonably large electromagnetic fields even when the configurations contain only negative dielectric materials with dissipation. This indicates a new line of approach for the design of plasmonic templates for enhanced processes like surface enhanced Raman scattering (SERS) and surface enhanced fluorescence apart from having enhanced nonlinear properties. Finally, while some authors consider a slab of NRIM as Alice's mirror [24], we may say localized electromagnetic fields in origami lenses behave in some way like the famous Alice's Cheshire cat who has the annoying habit of disappearing and appearing at random times and places. 'Well, I've often seen a cat without a grin', thought Alice, 'but a grin without a cat is the most curious thing I ever saw in my life'.

Acknowledgments

The authors acknowledge funding from the Indo-French Centre for Promotion of Advanced Research, New Delhi under grant no. 3804-02. SG is thankful for an ERC funding through ANAMORPHISM project no. 279673.

References

[1] Veselago V G 1968 *Sov. Phys.–Usp.* **10** 509
[2] Smith D R, Padilla W J, Vier V C, Nemat-Nasser S C and Schultz S 2000 *Phys. Rev. Lett.* **84** 4184
[3] Ramakrishna S A and Grzegorczyk T M 2009 *Physics and Applications of Negative Refractive Index Materials* (Boca Raton, FL: CRC Press)
[4] Pendry J B 2000 *Phys. Rev. Lett.* **85** 3966

[5] Smith D R, Schurig D, Rosenbluth M, Schultz S, Ramakrishna S A and Pendry J B 2003 *Appl. Phys. Lett.* **82** 1506–8
[6] O'Brien S, McPeake D, Ramakrishna S A and Pendry J B 2004 *Phys. Rev.* B **69** 241101
[7] Sersic I, Frimmer M, Verhagen E and Koenderink A F 2009 *Phys. Rev. Lett.* **103** 213902
[8] Soukoulis C M, Linden S and Wegener M 2007 *Science* **315** 47
[9] Pendry J B and Ramakrishna S A 2003 *J. Phys. Condens. Matter* **15** 6345
[10] Liu Y, Guenneau S, Gralak B and Ramakrishna S A 2013 *J. Phys.: Condens. Matter* **25** 135901
[11] Guenneau S, Vutha A C and Ramakrishna S A 2005 *New J. Phys.* **7** 164
[12] Chakrabart Si, Ramakrishna S A and Guenneau S 2006 *Opt. Express* **14** 12950
[13] Ramakrishna S A, Guenneau S, Enoch S, Tayeb G and Gralak B 2007 *Phys. Rev.* A **75** 063830
[14] Pendry J B 2004 *Contemp. Phys.* **45** 191
[15] Bliek P J, Deleuil R, Botten L C, McPhedran R C and Maystre D 1980 *IEEE Microwave Theory Tech.* **28** 1119
[16] Martin-Moreno L, Garcia Vidal F J, Lezec H J, Pellerin K M, Thio T, Pendry J B, Ebbesen T W 2001 *Phys. Rev. Lett.* **86** 1114
[17] Ramakrishna S A, Mandal P, Jeyadheepan K, Shukla N, Chakrabarti S, Kadic M, Enoch S and Guenneau S 2011 *Phys. Rev.* B **84** 245424
[18] Berenger J P 1994 *J. Comput. Phys.* **114** 185
[19] Bonnet-BenDhia A S, Ciarlet P and Zwolf C M 2010 *J. Comput. Appl. Math.* **234** 1912
[20] Fernandez-Dominguez A I, Maier S A and Pendry J B 2010 *Phys. Rev. Lett.* **105** 266807
[21] Movchan A B, Movchan N V, Guenneau S and McPhedran R C 2007 *Proc. R. Soc. Lond.* A **463** 1045
[22] Appel K, Haken W and Koch J 1977 *Illinois J. Math.* **21** 439
[23] Appel K and Haken W 1977 *Sci. Am.* **237** 108
[24] Lewis C 1995 *Alice in Wonderland* (New York: Gramercy Books)